



HAL
open science

Cateslytin abrogates lipopolysaccharide-induced cardiomyocyte injury by reducing inflammation and oxidative stress through toll like receptor 4 interaction

Carmine Rocca, Anna de Bartolo, Fedora Grande, Bruno Rizzuti, Teresa Pasqua, Francesca Giordano, Maria Concetta Granieri, Maria Antonietta Occhiuzzi, Antonio Garofalo, Nicola Amodio, et al.

► To cite this version:

Carmine Rocca, Anna de Bartolo, Fedora Grande, Bruno Rizzuti, Teresa Pasqua, et al.. Cateslytin abrogates lipopolysaccharide-induced cardiomyocyte injury by reducing inflammation and oxidative stress through toll like receptor 4 interaction. *International Immunopharmacology*, 2021, 94, pp.107487. 10.1016/j.intimp.2021.107487 . hal-03431855

HAL Id: hal-03431855

<https://hal.science/hal-03431855>

Submitted on 10 Mar 2023

HAL is a multi-disciplinary open access archive for the deposit and dissemination of scientific research documents, whether they are published or not. The documents may come from teaching and research institutions in France or abroad, or from public or private research centers.

L'archive ouverte pluridisciplinaire **HAL**, est destinée au dépôt et à la diffusion de documents scientifiques de niveau recherche, publiés ou non, émanant des établissements d'enseignement et de recherche français ou étrangers, des laboratoires publics ou privés.



Distributed under a Creative Commons Attribution - NonCommercial 4.0 International License

1 **Running title** Role of Cateslytin in Cardiomyocytes

2 **Cateslytin abrogates lipopolysaccharide-induced cardiomyocyte injury by reducing inflammation and**
3 **oxidative stress through toll like receptor 4 interaction**

4 Carmine Rocca^{#1}, Anna De Bartolo^{#1,2}, Fedora Grande³, Bruno Rizzuti⁴, Teresa Pasqua^{1,5}, Francesca
5 Giordano², Maria Concetta Granieri¹, Maria Antonietta Occhiuzzi³, Antonio Garofalo³, Nicola Amodio⁶,
6 Maria Carmela Cerra⁷, Francis Schneider^{8,9}, Maria Luisa Panno², Marie H el ene Metz-Boutigue^{9,10*} &
7 Tommaso Angelone^{1,11*}

8 ¹ Laboratory of Cellular and Molecular Cardiovascular Pathophysiology, Department of Biology, E and E.S., University
9 of Calabria, Rende, CS, Italy.

10 ² Department of Pharmacy, Health and Nutritional Sciences, University of Calabria, Rende, CS, Italy.

11 ³ Laboratory of Medicinal and Analytical Chemistry, Department of Pharmacy, Health and Nutritional Sciences,
12 University of Calabria, Rende, Italy.

13 ⁴ CNR-NANOTEC, Licryl-UOS Cosenza and CEMIF.Cal, Department of Physics, University of Calabria, Rende, Italy.

14 ⁵ Department of Health Science, University of Catanzaro Magna Graecia, 88100 Catanzaro, Italy.

15 ⁶ Department of Experimental and Clinical Medicine, Magna Graecia University of Catanzaro, Catanzaro, Italy.

16 ⁷ Laboratory of Organ and System Physiology, Department of Biology, E and E.S., University of Calabria, Rende, CS,
17 Italy.

18 ⁸ Department of Intensive Care, Hospital Hautepierre, University of Strasbourg, Strasbourg, France.

19 ⁹ Inserm UMR 1121, F ed eration de M edecine Translationnelle, University of Strasbourg, Strasbourg, France.

20 ¹⁰ Faculty of Odontology, University of Strasbourg, Strasbourg France.

21 ¹¹ National Institute of Cardiovascular Research (INRC), Bologna, Italy.

22

23 # These authors equally contributed to this work

24 **Corresponding Authors**

25 * Prof. Tommaso Angelone, University of Calabria, 87036 Arcavacata di Rende (CS), Italy. E-mail:
26 tommaso.angelone@unical.it

27 * Dr. Marie H el ene Metz-Boutigue, University of Strasbourg, Strasbourg, France. E-mail: marie-helene.metz@inserm.fr

29

30

31

32

33

34

35 **Abstract**

36 Global public health is threatened by new pathogens, antimicrobial resistant microorganisms and a rapid
37 decline of conventional antimicrobials efficacy. Thus, numerous medical procedures become life-threatening.
38 Sepsis can lead to tissue damage such as myocardium inflammation, associated with reduction of
39 contractility and diastolic dysfunction, which may cause death. In this perspective, growing interest and
40 attention are paid on host defence peptides considered as new potential antimicrobials. In the present study,
41 we investigated the physiological and biochemical properties of Cateslytin (Ctl), an endogenous
42 antimicrobial chromogranin A-derived peptide, in H9c2 cardiomyocytes exposed to lipopolysaccharide
43 (LPS) infection. We showed that both Ctl (*L* and *D*) enantiomers, but not their scrambled counterparts,
44 significantly increased cardiomyocytes viability following LPS, even if *L*-Ctl was effective at lower
45 concentration (1 nM) compared to *D*-Ctl (10 nM). *L*-Ctl mitigated LPS-induced LDH release and oxidative
46 stress, as visible by a reduction of MDA and protein carbonyl groups content, and by an increase of SOD
47 activity. Molecular docking simulations strongly suggested that *L*-Ctl modulates TLR4 through a direct
48 binding to the partner protein MD-2. Molecular analyses indicated that the protection mediated by *L*-Ctl
49 against LPS-evoked sepsis targeted the TLR4/ERK/JNK/p38-MAPK pathway, regulating NFkB p65, NFkB
50 p52 and COX2 expression and repressing the mRNA expression levels of the LPS-induced proinflammatory
51 factors IL-1 β , IL-6, TNF- α and iNOS. These findings indicate that Ctl could be considered as a possible
52 candidate for the development of new antimicrobials strategies in the treatment of myocarditis. Interestingly,
53 *L*-enantiomeric Ctl showed remarkable properties in strengthening the anti-inflammatory and anti-oxidant
54 effects on cardiomyocytes.

55 **Keywords**

56 Cardiomyocytes, Cateslytin, Antimicrobial Peptides, Inflammation, Oxidative Stress, Toll-like receptor 4

57

58

59

60

61

62

63

64

65

66

67 **1. Introduction**

68 Evidences from epidemiological studies conducted on post-mortem individuals identified myocarditis as a
69 significant cause of unexpected death, representing a major reason of cardiovascular events. Myocarditis is a
70 potentially life-threatening disease and mostly occurs in young and adult people [1]. Accordingly, biopsy-
71 proven myocarditis was reported in 9–16% of adult patients and a prevalence of myocarditis of 2-42% of
72 cases in young people was registered [1 and references therein]. Several viral and bacterial infections
73 represent etiological agents of myocarditis. Among them, the severe acute respiratory syndrome coronavirus
74 2 (SARS-CoV-2) can cause myocarditis as evinced by numerous recent investigations reporting cases of
75 acute myocarditis or myocardial inflammation in coronavirus disease 2019 (COVID-19) [2,3 and references
76 therein]. Also, direct infection of the heart muscle by bacteria and bacteria-produced toxins can be
77 responsible of myocarditis and severe myocardial damage. Bacterial myocarditis is usually observed in the
78 context of a severe sepsis, such as an infection induced by Gram-negative bacteria, that can lead to multi-
79 organ failure, including heart dysfunction and arrhythmias that can occur in around 60% of septic patients
80 [4]. Clinical and experimental studies have extensively reported how decreased contractility and impaired
81 myocardial compliance constitute major factors causing myocardial dysfunction in sepsis [5].

82 Lipopolysaccharide (LPS) represents the major component of the outer membrane of Gram-negative bacteria
83 that belongs to the pathogen-associated molecular patterns (PAMPs). During myocardial inflammation, LPS
84 interacts with the key member of pattern-recognition receptors (TLRs), the toll-like receptor 4 (TLR4),
85 expressed on the surface of host cardiomyocyte, stimulating the innate immune system and inducing the
86 inflammatory response [6]. TLR4 activation by LPS induces the myeloid differentiation factor 88 (Myd88)-
87 dependent pathway, converging on nuclear transcription factors activation, such as nuclear factor- κ B
88 (NF κ B). This, in turn, induces the production of pro-inflammatory cytokines leading to inflammatory
89 cascades that are associated with several cardiovascular diseases, including myocarditis and heart failure [7
90 and references therein].

91 The identification of new classes of drugs to include in the therapeutic options for inflammatory dilated
92 cardiomyopathy and myocarditis, for which the availability of specific treatment remains limited, is of
93 crucial clinical interest. This is particularly important also given the global increasing impact of antibiotic-
94 resistant infections on health and economic outcomes [8]. In this context, antimicrobial peptides (AMPs) are
95 antimicrobial agents active against infections that do not show the typical disadvantages of more
96 conventional antibiotics related to possible gastrointestinal or allergic reactions, and associated to antibiotic-
97 resistant bacteria [9].

98 Chromogranin A (CgA), a member of the chromogranin/secretogranin family, is a pro-hormone localized in
99 the secretory vesicles of neurons, neuroendocrine cells, granulocytes, immune cells and cardiomyocytes [10-
100 12]The intravesicular proteolytic processing of CgA under physiological or stress conditions generates
101 several protein fragments with different biological activities [12], ranging from the regulation of innate
102 immunity, antimicrobial activities and inflammation to neuroprotection and cardiovascular protection

103 [13,14,15]. One of the CgA cleavage products, the bioactive peptide Catestatin (Cst, human CgA₃₅₂₋₃₇₂) was
104 initially described as a potent inhibitor of catecholamines release via the nicotinic receptor [16].
105 Experimental evidences report that Cst may affect the heart function and the blood pressure both directly and
106 indirectly, playing a crucial regulatory role in cardiovascular system under physiological and pathological
107 conditions [13,17]. Accordingly, Cst is able to counteract the cardiac effects following adrenergic
108 stimulation, and to protect the heart against ischemia/reperfusion injury, acting as a post-conditioning
109 protective agent [13]. It is also known that Cst contributes to the immune system regulation and can mitigate
110 severe inflammatory response, thus preserving tissues function [17].

111 In addition to several other AMPs resulting from the natural processing of CgA, such as vasostatin-1, the
112 core sequence of Cst, Cateslytin (Ctl; bovine CgA₃₄₄₋₃₅₈, with sequence RSMRLSFRARGYGFR), can also
113 act as host defense peptides (HDPs), due to its antimicrobial activities against a wide number of pathogens
114 [18]. In addition, compared to other CgA fragments with antimicrobial properties, Ctl is able to resist to the
115 degradation when treated with bacterial supernatants [19] and it is unable to induce resistance for the host
116 [20].

117 Based on these knowledges, the present work was undertaken to explore: i) the ability of the two
118 enantiomers of the Ctl (*L* or *D* amino acids) to mitigate the cardiomyocyte injury evoked by LPS infection;
119 ii) the potential ability of *L*-Ctl to affect TLR4 through interaction with the partner protein MD-2; iii) the
120 molecular mechanism of action underlying the effect of *L*-Ctl in the presence of LPS in H9c2
121 cardiomyocytes.

122

123 **2. Material & Methods**

124 **2.1. Peptides and chemicals**

125 *L*-Ctl (CgA₃₄₄₋₃₅₈, RSMRLSFRARGYGFR) and its derivate *D*-Ctl were synthesized by Proteogenix SAS
126 (Schiltigheim, France) according to the Merrifield Technique, a stepwise solid-phase peptide synthesis
127 approach with Fmoc chemistry, and purified to >95% by using reverse phase high-performance liquid
128 chromatography (RP-HPLC) and controlled by MALDI-TOF mass spectrometry. As negative controls, the
129 scrambled *L*-Ctl and *D*-Ctl (FMRLRYRSSAFGGRR, in *L*- and *D*-aminoacid forms, respectively) have been
130 used. Both *L*-Ctl and *D*-Ctl were dissolved in sterile water before use (UltraPure RNase/DNase-free distilled
131 water, Invitrogen, California, USA). Lipopolysaccharides (LPS) from *Escherichia coli* O55:B5, sodium
132 pyruvate and β -nicotinamideadenine dinucleotide disodium salt, 2,4 dinitrophenylhydrazine (DNPH), 2-
133 thiobarbituric acid (TBA), bovine serum albumin (BSA), butanol-1, butylated hydroxyanisole, diethyl ether,
134 ethylenediaminetetraacetic acid (disodium salt), streptomycin sulfate, tween-20 and urea were obtained from
135 Sigma Aldrich (St. Louis, MO, USA). Dimethyl sulfoxide (DMSO) was purchased from PanReac
136 AppliChem (Glenview, Illinois, USA). Absolute ethanol, ethyl acetate, hydrochloric acid, methanol and
137 trichloroacetic acid were purchased from Carlo Erba Reagents (Cornaredo, MI, Italy).

138

139 **2.2. Cell culture**

140 H9c2 cells (rat embryonic cardiomyocytes) were obtained from American Type Culture Collection (ATCC,
141 Manassas, VA, USA) (Cat# CRL-1446_H9c2, RRID:CVCL_0286) and maintained in Dulbecco's Modified
142 Eagle Medium/Nutrient Mixture F-12 (DMEM/F-12, Gibco, Thermo Fisher Scientific, Waltham, MA, USA)
143 containing 10% fetal bovine serum (FBS, Gibco) and supplemented with 1% penicillin/streptomycin
144 (Thermo Fisher Scientific), incubated at 37°C in humidified atmosphere with 5% CO₂ [21]. When the cells
145 reached a density of 80% in 100-mm dishes, they were digested using 0.25% Trypsin-EDTA (1X) (Gibco)
146 according to a 1:2 ratio following manufacturer's instructions (ATCC). For each experiment, the cells were
147 seeded and incubated for 48 h at 37°C, 95% O₂ and 5% CO₂.

148 **2.2.1. Cell viability assay**

149 H9c2 cell viability was evaluated by 3-(4,5-dimethylthiazol-2-yl)-5-diphenyl tetrazolium bromide (MTT)
150 assay, as previously described [21]. The cells were seeded at a density of 5×10³ cells/well in 96-well plate
151 and exposed to the following treatments: Control (vehicle), *L*-Ctl (from 1 to 100 nM), *D*-Ctl (from 1 to 100
152 nM), LPS (10 µg/mL) alone, LPS + *L*-Ctl (from 1 to 100 nM), LPS + *D*-Ctl (from 1 to 100 nM), LPS +
153 scrambled *L*-Ctl (from 1 to 100 nM) and scrambled *L*-Ctl (from 1 to 100 nM) for 6 h [22]. The control was
154 treated with the vehicle (UltraPure RNase/DNase-free distilled water). At the end of the treatments, the cell
155 culture medium was replaced with 100 µl of 2 mg/ml MTT solution (Sigma Aldrich) and the cells were
156 incubated for 4 h at 37°C, 5% CO₂. After incubation, the solution was removed and the formazan crystals
157 were solubilized by adding 100 µl of DMSO for 30 min. The absorbance was measured using a Multiskan
158 EX Microplate Reader Lab (Thermo Fisher Scientific) at 570 nm. The means of absorbance values of six
159 wells in each experimental group were expressed as the percentage of cell viability. The experiment was
160 repeated three independent times. Cell viability were reported as percentage of cells survival relative to
161 control cells.

162 **2.2.2. Biochemical analyses of H9c2 cells**

163 **2.2.2.1. Lactate dehydrogenase (LDH) activity determination**

164 The structural integrity of cultured H9c2 cardiomyocytes was evaluated by determining the level of LDH
165 released in the culture supernatant. To this aim, the cells were seeded in a 24-well plate at a density of 1 ×
166 10⁵ cell/ml and treated with vehicle (control), LPS (10 µg/mL), LPS + *L*-Ctl (1 nM) and *L*-Ctl (1 nM) alone
167 for 24 h. 100 µl of the culture supernatant per well was used for LDH activity determination. The enzyme
168 activity was evaluated spectrophotometrically (GENESYS 20 spectrophotometer, Thermo Fisher Scientific),
169 following the method of McQueen (1972) [23]. After incubation of reagents, absorbance at 340 nm was
170 recorded every min until steady-state was reached. The reaction velocity was determined by a decrease in

171 absorbance at 340 nm, resulting from the oxidation of NADH indicative of LDH activity, that was expressed
172 in IU/L [24].

173

174

175 **2.2.2.2. Evaluation of malondialdehyde (MDA) concentration**

176 The concentration of MDA (as an indicator of lipid peroxidation following ROS generation) in H9c2 cell
177 lysates was determined by thiobarbituric acid reactive substances (TBARS) assay, as previously described
178 [25-27]. The cells were seeded in a 24-well plate at a density of 1×10^5 cell/ml and treated as described
179 above for 6 h. Subsequently, cells were washed with cold phosphate buffered saline (PBS), centrifuged at
180 $300 \times g$ for 10 min and the supernatant was removed. The precipitate obtained was resuspended in 1 mL of a
181 cold sodium phosphate buffer 10 mM (containing 1 mM ethylenediaminetetraacetic acid and 1 mM butylated
182 hydroxyanisole in 0.15 % ethanol), pH = 7.2 and crushed by ultrasonic wave. MDA concentration was
183 estimated spectrophotometrically (GENESYS 20 spectrophotometer, Thermo Fisher Scientific). The
184 absorbance difference A (535–600 nm) was converted to MDA equivalents using the extinction coefficient
185 for MDA $1.55 \times 10^5 \text{ M}^{-1}\text{cm}^{-1}$. Lipid peroxidation was expressed in mM MDA.

186 **2.2.2.3. Estimation of protein carbonyl content**

187 The assessment of the protein carbonyl content (as an indicator of protein damage following oxidative stress)
188 was evaluated in H9c2 cells by 2,4 dinitrophenylhydrazine (DNPH) assay, following the method of Reznick
189 and Packer (1994) [28] and as previously described [26, 27]. Cells were seeded in a 24-well plate at a density
190 of 1×10^5 cell/ml and treated as described above for 6 h. Subsequently, they were washed with cold PBS,
191 centrifuged at $300 \times g$ for 10 min and the supernatant was removed. The precipitate obtained was
192 resuspended in 1 mL of a cold phosphate buffer 50 mM, pH 6.7, containing 1 mM
193 ethylenediaminetetraacetic acid and crushed by ultrasonic wave. The protein carbonyl content (expressed in
194 μM) was evaluated spectrophotometrically (GENESYS 20 spectrophotometer, Thermo Fisher Scientific) by
195 absorbance detected at 375 nm, using the extinction coefficient for DNPH ($22 \text{ mM}^{-1} \text{ cm}^{-1}$).

196 **2.2.2.4. Superoxide dismutase (SOD) enzyme activity assay**

197 SOD activity was determined by measuring the inhibition of pyrogallol autoxidation following the method of
198 Marklund S. and Marklund G. (1974) [29] and as previously described [30]. The cells were seeded in a 24-
199 well plate at a density of 1×10^5 cell/ml and treated as described above for 6 h. Subsequently, the cells were
200 washed with cold PBS, centrifuged at $300 \times g$ for 10 min and the supernatant was removed. The precipitate
201 obtained was resuspended in Tris buffer 50 mM, pH 8.2, containing 100 mM ethylenediaminetetraacetic acid
202 and the reaction was initiated by adding 8 mM pyrogallol (prepared in 1 mM HCl). The SOD activity in the
203 cell extract was measured by monitoring the autoxidation of pyrogallol for 5 min at room temperature using

204 a GENESYS 20 spectrophotometer (Thermo Fisher Scientific) at 420 nm. SOD activity was assessed as the
205 degree of inhibition of the pyrogallol autoxidation rate.

206 **2.2.3. Western blot**

207 At the end of treatments with vehicle (control), LPS (10 µg/mL), LPS + *L*-Ctl (1 nM) and *L*-Ctl (1 nM)
208 alone, the H9c2 cardiomyocytes were washed with DPBS (Gibco) and the proteins were extracted using
209 RIPA lysis buffer (Sigma Aldrich) suitably supplemented with a mixture of protease inhibitors [(aprotinin 20
210 µg/mL, phenylmethylsulfonyl fluoride 1%, sodium orthovanadate 2 µM (Sigma-Aldrich)]. Cells were
211 scraped and transferred in microcentrifuge tubes, incubated on ice for 30 min with intermittent mixing, and
212 then centrifugated at 12,000 *g* for 15 min at 4°C. The supernatant was collected for protein concentration
213 determination by Bradford reagent using bovine serum albumin (BSA) as a standard. Equal amounts of
214 protein (30 µg) were loaded on 10% SDS-PAGE gel [for toll like receptor 4 (TLR4), **phospho-extracellular-**
215 **signal-regulated kinase 1/2 (p-ERK1/2), ERK1/2, phospho-c-Jun N-terminal kinase 1/2 (p-JNK1/2), JNK1/2,**
216 **p-p38 mitogen-activated protein kinase (p-p38 MAPK), nuclear factor kappa-light-chain-enhancer of**
217 **activated B cells (NFkB) p52, p-NFkB p65, NFkB p65** and cyclooxygenase-2 (COX2)], exposed to
218 electrophoresis, and transferred to polyvinyl difluoride membranes (GE Healthcare, Chicago, USA).
219 Membranes were blocked in 5% non-fat dried milk at room temperature for 1 h, and then incubated
220 overnight at 4°C with primary antibodies specific for the above antigens diluted 1:1000 (for TLR4, **p-**
221 **ERK1/2 and ERK1/2**) or 1:500 (for **p-JNK1/2, JNK1/2, p-NFkB p65, NFkB p65, NFkB p52** and COX2) in
222 tris-buffered saline containing 0.2% Tween 20 (TBST) and 5% BSA.

223 Antibodies against β-actin, **ERK1/2, JNK1/2, p38-MAPK and NFkB p65** were used as internal controls.
224 Following incubation with primary antibodies, all membranes were washed three times with TBST for 5 min
225 and then incubated with secondary antibodies at room temperature for 2 h (anti-mouse and anti-rabbit
226 peroxidase-linked, Santa Cruz Biotechnology, California, USA), diluted 1:2000 in TBST containing 5% non-
227 fat dried milk. Immunodetection was carried out using the enhanced chemiluminescence kit (GE Healthcare).
228 Membranes were exposed to X-ray films (Hyperfilm ECL, Amersham), the densitometric analyses of the
229 bands areas and the pixel intensity were performed and the background was subtracted. The analyses were
230 carried out using ImageJ 1.6 (National Institutes of Health, Bethesda, Maryland) as previously described
231 [31,32].

232

233 **2.2.4. Molecular docking**

234 The molecular docking engine Autodock Vina [33] was used to simulate the binding of *L*-Ctl to the myeloid
235 differentiation protein 2 (MD-2), the partner protein of TLR4. The structure of MD-2 was extracted from the
236 entry 4G8A of the Protein Data Bank [34], which reports the crystallographic conformation of the complex
237 with human TLR4 (polymorphic variant D299G and T399I) and with several ligand species in the binding
238 site. All these molecules, including crystallographic waters, were not considered in the docking. Human Ctl

239 (sequence SSMRLSFRARGYGFR, L-enantiomeric form) was built in extended conformation by using
240 UCSF Chimera [35].

241 Since the conformational space of Ctl is too large to be explored in a single simulation run, the search was
242 performed in a simplified way, in analogy with a protocol already described for simulating the docking of
243 peptides [36,37]. Full flexibility was guaranteed to seven consecutive residues [38], and the internal degrees
244 of freedom of the other eight were inhibited. The flexible region was then systematically varied along the
245 peptide sequence, from the N to the C terminus (SSMRLSF, SMRLSFR, ..., ARGYGFR), for a total of nine
246 distinct simulations. The search was performed in a volume ($40 \text{ \AA} \times 40 \text{ \AA} \times 40 \text{ \AA}$) larger than the binding site
247 of MD-2, and with exhaustiveness much greater (8-32 times larger) than the default value [39,40].

248

249 **2.2.5. Quantitative Reverse-Transcription Real-Time PCR (qRT-PCR)**

250 H9c2 cells were grown in 6-well plate to 70-80% confluence and then treated with vehicle (control), LPS (10
251 $\mu\text{g/mL}$), LPS + *L*-Ctl (1 nM) and *L*-Ctl (1 nM) alone. Total RNA from cells was isolated using TRIzol
252 reagent (Invitrogen, Life Technologies, Carlsbad, CA, USA) according to the manufacturer's protocol. The
253 purity and integrity of RNA were confirmed by spectrophotometric analysis.

254 1 μg of total RNA was reverse transcribed to provide complementary DNA (cDNA) using High-Capacity
255 cDNA Reverse Transcription Kit (Applied Biosystems™, Thermo Fisher Scientific). The cDNA was
256 amplified by qRT-PCR using SYBR™ Select Master Mix (Thermo Fisher Scientific) according to the
257 manufacturer's instructions on Applied Biosystems™ QuantStudio™ 5 Real-Time PCR System apparatus
258 (Thermo Fisher Scientific). Samples were analyzed in triplicate (n=3 independent experiments) and the
259 relative mRNA expression levels of the different genes were normalized to rRNA18S and calculated on the
260 basis of the $2^{-\Delta\Delta C_t}$ method [41,42].

261 Primers used for the amplification were: forward 5'-CCCAGGACATGCTAGGGAGCC-3' and reverse 5'-
262 AGGCAGGGAGGGAAACACACG-3' (IL-1 β); forward 5'-TGGAGTTCCGTTTCTACCTGG-3' and
263 reverse 5'-GGTCCTTAGCCACTCCTTCTGT-3' (IL-6); forward 5'-CACCACGCTCTTCTGTCTACTG-3'
264 and reverse 5'-GCTACGGGCTTGTCACCTCG-3' (TNF- α); forward 5'-AGCCCTCACCTACTTCCTGG-3'
265 and reverse 5'-CTCTGCCTGTGCGTCTCTTC-3' (NOS2); forward 5'-GCAATTATCCCCATGAACG-3'
266 and reverse 5'-GGCCTCACTAAACCATCCAA-3' (18S).

267

268 **2.2.6. Statistical Analysis**

269 Data, expressed as mean \pm SEM, were analysed by one-way ANOVA and the non-parametric Newman-
270 Keuls Multiple Comparison Test (for post-ANOVA comparisons) and one-way ANOVA followed by
271 Dunnett's Multiple Comparison Test when appropriate. Values of *p = <0.05, **p = <0.01, ***p = <0.001
272 were considered statistically significant. The statistical analysis was carried out using Graphpad Prism 5
273 (GraphPad Software, La Jolla, California, USA).

274 **3. Results**

275 **3.1. Effect of *L*-Ctl and *D*-Ctl on cell proliferation in H9c2 cardiomyocytes**

276 In order to evaluate the effects of catestatin-derived peptides, *L*-Ctl and *D*-Ctl, on cell viability, H9c2 cells
277 were exposed to increasing concentrations of either peptide species and the MTT was performed. As shown
278 in **Figure 1A**, *L*-Ctl induced a significant increase in cell proliferation to each concentration tested (1-100
279 nM), while *D*-Ctl produced a significant increase in cardiac cell viability only at 5 nM, 10 nM and 100 nM
280 (**Figure 1B**).

281

282 **3.2. Action of *L*-Ctl and *D*-Ctl on LPS-induced damage in H9c2 cells**

283 The action of *L*-Ctl or *D*-Ctl on LPS-induced injury in H9c2 cardiac cells was then investigated. To this aim,
284 the cells were treated with LPS alone and in combination with increasing concentrations of *L*-Ctl or *D*-Ctl
285 and cell viability was evaluated (**Figure 2**). MTT revealed that the treatment with LPS was able to
286 significantly reduce cardiomyocytes viability; however, the cytotoxic effect exerted by LPS was reversed by
287 both *L*-Ctl (**Figure 2A**) and *D*-Ctl (**Figure 2B**) treatments. In particular, *L*-Ctl induced beneficial effects on
288 LPS-dependent cytotoxicity starting from 1 nM, and its effect was significant at each concentration tested
289 (up to 100 nM) (**Figure 2A**). In contrast, *D*-Ctl reduced the H9c2 mortality when co-administered with LPS,
290 only in the concentration range 10-100 nM (**Figure 2B**). Scrambled *L*-Ctl and *D*-Ctl were used as negative
291 controls. **Figure 3** indicates that scrambled *L*-Ctl was inactive, since no significant effects have been
292 observed on viability of H9c2 cells at the concentrations range of 1-100 nM, in the absence (**Figure 3A**) or
293 in the presence of LPS (**Figure 3B**). Comparable data were obtained with the scrambled *D*-Ctl (data not
294 shown).

295 **3.3. Influence of *L*-Ctl on TLR4 expression in LPS-stimulated H9c2**

296 Among the two Ctl enantiomers, *L*-Ctl has been showed to be more active (1 nM, that is referred to the first
297 effective concentration) compared to *D*-Ctl (10 nM, that is referred to the first effective concentration) in the
298 presence of LPS. Therefore, the cardiac molecular mechanism of *L*-Ctl was investigated. Western blot and
299 densitometric analyses of cell extracts showed that TLR4 expression was significantly increased in LPS-
300 treated cells with respect to the control group, whereas in the LPS + *L*-Ctl group the protein expression was
301 reduced (**Figure 4**).

302 **3.4. Molecular docking**

303 Molecular docking was used to investigate whether the presence of *L*-Ctl can affect TLR4. Bacterial
304 lipopolysaccharide and its precursor lipid A, as well as peptidomimetics with no structural similarity to the
305 physiological ligands of TLR4, do not bind this protein directly but anchor in the relatively large binding site
306 of its co-receptor MD-2 [34,43]. The conformation of MD-2 is similar in all these complex, and they only
307 differ by the molecular contacts formed with the various ligands. Thus, we performed the molecular docking

308 of *L*-Ctl to a monomer of MD-2 extracted from a complex with human TLR4 [34], and isolated from any
309 other molecular species.

310 Ctl possesses 15 amino acid residues and 64 rotatable dihedral angles, which is a number far too large to be
311 exhaustively explored in a single molecular docking run. Therefore, the conformational space of the peptide
312 was explored in a simplified way, by allowing rotations in the main and side chains of seven consecutive
313 residues while the other eight residues were considered rigid, and systematically varying such flexible region
314 along the whole peptide sequence.

315 The results indicated that the central region of *L*-Ctl (sequence fragment LSFRRARG) has the most favorable
316 affinity for MD-2, with a predicted binding energy of -10 kcal/mol. In contrast, the two peptide endings
317 showed a comparatively lower binding score, with -8 kcal/mol for the N-terminal region and -8.5 kcal/mol
318 for the C-terminal one. Due to the fact that the rigid portion of peptide structure was not optimized in the
319 simulations, these values should be considered as an upper limit for the (negative) binding energy, and may
320 reflect an even more favorable binding. The overall findings suggest a high affinity of *L*-Ctl for MD-2, with
321 a binding equilibrium constant in the nanomolar range. **Figure 5** shows the structure or the most favorable
322 docking pose of *L*-Ctl to MD-2 obtained in the simulations. The peptide is deeply inserted in the core of the
323 protein binding site, and its position mostly overlaps with the location of the physiological ligands [34] in the
324 original crystallographic complex.

325 **3.5. Involvement of inflammatory pathways in *L*-Ctl mechanism of action**

326 Western blot and densitometric analyses of H9c2 cell extracts were carried out to determine the expression
327 levels of p-ERK1/2 (**Figure 6A**), p-JNK1/2 (**Figure 6B**), p-p38 MAPK (**Figure 6C**), NFkB p65 (**Figure**
328 **6D**), NFkB p52 (**Figure 6E**) and COX2 (**Figure 6F**) in H9c2 cells treated with LPS in the presence or
329 absence of *L*-Ctl. The expression of all the above proteins significantly increased following LPS treatment
330 and significantly decreased in the cells treated with LPS + *L*-Ctl (**Figure 6**).

331 **3.6. Effect of *L*-Ctl on mRNA expression levels of inflammatory mediators**

332 The *L*-Ctl molecular effect on the LPS-injured H9c2 cells was further investigated by assessing the mRNA
333 expression levels of selective inflammatory mediators. qRT-PCR analysis of cell extracts revealed that the
334 proinflammatory factors IL-1 β (**Figure 7A**), IL-6 (**Figure 7B**), TNF- α (**Figure 7C**) and NOS2 (iNOS)
335 (**Figure 7D**) were significantly upregulated in LPS-stimulated H9c2 cells compared with the control group.
336 On the contrary, the mRNA expression levels of the above markers were significantly reduced in LPS + *L*-
337 Ctl experimental group.

338 **3.7. Effect of *L*-Ctl on oxidative stress-related markers, SOD activity and LDH release in H9c2** 339 **exposed to LPS**

340 To determine whether *L*-Ctl could affect the cellular oxidative balance under LPS treatment, oxidative stress-
341 related markers and the activity of the antioxidant enzyme SOD were measured. The MDA production and

342 the content of protein carbonyl groups, used as lipid peroxidation and protein damage markers, respectively,
343 were assayed in H9c2 cell lysates. **Figure 7** shows that MDA concentration (**Figure 7A**) and protein
344 carbonyl groups content (**Figure 7B**) were significantly increased in LPS group compared to the control,
345 while they were significantly decreased in the LPS + *L*-Ctl co-treatment. On the contrary, the percentage of
346 pyrogallol autoxidation (i.e. index of SOD activity) was significantly decreased in LPS-exposed H9c2, and
347 significantly increased in the LPS + *L*-Ctl group (**Figure 7C**). *L*-Ctl alone did not exert significant effects on
348 the above parameters compared to the vehicle exposed cells (**Figure 7 A-C**). As depicted in **Figure 7D**, LPS
349 treatment also significantly increased LDH, whose release in the H9c2 culture medium is considered an
350 indicator for cell membrane damage, whereas the co-treatment with *L*-Ctl reversed, to a significant extent,
351 the enzyme concentration released in response to LPS. *L*-Ctl treatment alone did not induce significant effect
352 in the LDH release compared to the control group (**Figure 7D**).

353 4. Discussion

354 The present study aimed to investigate the possible protective effects of Ctl in LPS-stimulated H9c2
355 cardiomyocytes. For the first time, we demonstrated that both *L*-Ctl and *D*-Ctl significantly increase cell
356 viability under LPS stimulation. Since the *L*-enantiomeric form of the peptide resulted more effective, it was
357 used for the subsequent analyses of the underlying mechanism of action. Our simulation results suggested
358 that Ctl may influence the biological activity of TLR4 through a direct binding to the partner protein MD-2.
359 In addition, molecular analyses showed that *L*-Ctl mitigates the LPS-dependent oxidative stress, the
360 reduction of SOD activity and the release of LDH in the cell medium. The peptide is also able to **decrease the**
361 **expression of inflammatory signaling molecules (IL-1 β , IL-6, TNF- α , iNOS) and the activation of important**
362 **inflammatory mediators (p-ERK 1/2, p-JNK, p-p38 MAPK, p-NF κ B p65, p-NF κ B p52, COX2).** These data
363 are of interest in the context of myocarditis and in the field of antimicrobial peptides (AMPs) in regard to
364 their capability to counteract antibiotic resistance.

365 Antibiotic resistance, primarily due to the overuse of these drugs, has emerged as a severe worldwide health
366 problem, as every year millions of people are affected by multi-drug resistant bacteria resulting in a high
367 case-fatality ratio. For this reason, growing energies and efforts are invested in this field trying to reduce
368 antibiotic prescription and to identify or design alternative drugs able to overcome resistance. Among the
369 molecules currently considered as novel anti-infective agents [44], a prominent position is occupied by
370 AMPs, major players in the innate defense, since they have a relatively low chance to establish resistance
371 [45]. AMPs exist across all major lineages, they represent highly conserved forms of innate immunity and
372 are active against numerous pathogens [46]. Their short amphipathic -cationic conformation seems to be a
373 key component of their antimicrobial activity, since it promotes the disruption of microbial membranes [47].
374 In particular, mammalian AMPs are able to directly kill the microbe and activate rapidly the immune
375 response [48].

376 Ctl, the shorter and active arginine rich N-terminus fragment of CgA-derived Cst peptide, can be fully
377 included among AMPs, being effective against many microbial strains [18-20]. In the present study we tested

378 on an *in vitro* model of myocarditis, i.e. LPS-stimulated H9c2 cells [49], both the naturally occurring
379 enantiomeric species *L*-Ctl and its derived eptideptide *D*-Ctl, where all *L*-amino acids have been replaced by
380 *D*-amino acids. In this regard, it is known that LPS, expressed on the external membrane of Gram-negative
381 bacteria, represents a powerful inducer of immunity responses through the modulation of toll-like receptors 4
382 (TLR4) [7]; for this reason, it is widely used to reproduce inflammatory diseases, such as myocarditis [50].
383 Myocarditis, or inflammatory cardiomyopathy, is an inflammatory condition of the myocardium that, if
384 prolonged, leads to cardiac injury, cardiac dysfunction, cardiomyocytes death [49] and resistance of the
385 infectious agents to therapies [51].

386 In our experimental model, both *L*-Ctl and *D*-Ctl were able to improve cell viability, alone or when
387 administered together with LPS, while their scrambled *L*-Ctl and *D*-Ctl counterparts were unable to
388 significantly affect cell viability. Indeed, according to previous data [52], LPS alone reduces cell viability
389 and induces a significant release of LDH (an indicator of cytotoxicity) in the culture medium, indicating that
390 the model of myocarditis has been successfully established. Of note, *L*-Ctl showed greater effectiveness with
391 respect to the *D*-enantiomeric form in increasing cell viability and in relieving LPS effects at all the tested
392 concentrations. *D*-Ctl was produced, starting from its natural peptide, to promote the stability of the peptide
393 against bacterial proteases and, at variance with our results, it was much more effective against microbial
394 strains and more resistant to proteolytic degradation than *L*-Ctl [18,20]. Nevertheless, our study did not
395 include a microbiology approach but aimed to analyze an *in vitro* model of myocarditis and this may account
396 for the different potency observed for *D*-Ctl and *L*-Ctl in these diverse experimental sets. Moreover, it is
397 conceivable that, from a physiological point of view, H9c2 cells establish a more favorable interactions with
398 the natural occurring *L*-Ctl, since molecular chirality is a key feature in molecular host-guest recognition
399 [53]. Results have been further corroborated by the use of a scrambled/inert peptide.

400 Thus, we focused on the anti-bacterial/anti-inflammatory role of *L*-Ctl possibly mediated via the TLR4
401 pathway. It is well established that LPS activates TLR4 and its downstream cascade by the interaction with
402 its essential accessory protein, namely MD-2 [54]. LPS binds the hydrophobic pocket of MD-2 through 5 of
403 its acyl chains, allowing the engagement and the dimerization of TLR4 and the generation of the activated
404 LPS-MD2-TLR4 complex [54]. The crucial role of MD-2 in TLR4 inflammatory responses has been
405 supported by studies performed on MD-2 knockout mice, that showed hypo-responsiveness to LPS and
406 higher rate of survival to endotoxic shock [55]. Confirming previous experimental evidences, in our model
407 LPS induces an increase in TLR4 protein expression, generally regulated by transcriptional and post-
408 transcriptional mechanisms [56]. This supports the important contribution of TLR4 to the relationship
409 existing between inflammation and cardiovascular disorders. Since *L*-Ctl was able to mitigate the LPS-
410 dependent upregulation of TLR4, it is conceivable that a regulation of its expression at the MD-2 level may
411 exist. Accordingly, the molecular docking analysis clearly supported the interaction between the peptide and
412 MD-2, the TLR4 partner protein. Indeed, the results of our computational studies suggest a high affinity of
413 *L*-Ctl for MD-2, with a predicted binding energy of at least -10 kcal/mol. The peptide deeply plunged into

414 the protein binding site with residues Phe7, Arg8 and Arg10. It is likely that the energetic penalty due to the
415 desolvation of the arginine side chains buried into the protein pocket was adequately compensated by
416 electrostatic and entropic effects at the peptide termini, which are exposed and relatively free to fluctuate in
417 the solvent, although such effects cannot be directly assessed by using molecular docking. A number of
418 interactions stabilized the anchoring of the peptide into MD-2, including electrostatic attraction with the
419 charged residue Glu92 of the protein, and hydrophobic interactions with several phenylalanine isoleucine
420 residues. Thus, our simulation results strongly suggest the possibility that Ctl may influence the biological
421 activity of TLR4 through a direct binding to the partner protein MD-2. Both the interaction energy and the
422 predicted location of binding of Ctl are fully consistent with an anchoring in the protein pocket, similar to the
423 one observed in the experiment for physiological ligands bound to MD-2. The interaction between Ctl and
424 MD-2 could thus represent the mechanism used by the peptide to suppress LPS inflammation, since a
425 competitive antagonism on this site can be postulated.

426 **It is widely accepted that the activation of TLR4, such as under LPS stimulation, induces the downstream**
427 **MAPKs cascade converging on NFkB, lastly able to promote the expression of pro-inflammatory actors,**
428 **including IL-1 β , IL-6, TNF- α , NOS2 [57,58]. Of note, Ctl downregulates the expression of these proteins**
429 **corroborating its supposed anti-inflammatory action via TLR4 inhibition.**

430 Moreover, it is known that NFkB importantly participates in immune responses [59] and its overactivation
431 contributes to the long-term inflammation responsible for acute myocardial lesions [60]. Indeed, NFkB is a
432 well established downstream **player** of LPS/TLR4, **MAPKs and JNK** activation [56,61,62], and a positive
433 regulator of COX2 expression, a key enzyme of inflammatory pathways [63]. Accordingly, our results
434 showed an increase of **p-ERK 1/2, p-JNK, p-NFkB p65, p-NFkB p52**, and inducible COX under LPS
435 stimulation, reversed by the addition of *L*-Ctl to the medium. Therefore, it is plausible that *L*-Ctl, by reducing
436 the LPS-induced NFkB expression, may **also** prevent the production and the release of proinflammatory
437 cytokines in cardiac myocytes [64], **as showed in our experimental set**. This finding can be further supported
438 by evidences indicating the ability of another CgA-derived peptide (chromofungin, CgA₄₇₋₆₆) to exert
439 antiinflammatory effects by inhibiting the NFkB-mediated transcription [65]. Interestingly, in our LPS-
440 stimulated model **p38 MAPK** is more phosphorylated, according to the increased expression of NFkB,
441 conversely to what happens under Ctl treatment. **Being NFkB a crucial target for MAP-kinases, such as p38**
442 **MAPK that is strongly involved in cardiac pathologies [66 and references therein], this result may be useful**
443 **in the view of future frontiers in therapeutics.**

444 Another important aspect regards the well established ROS production, and its resulting oxidative stress,
445 detectable in septic myocardial inflammation [67,68]. According to these data, in our model LPS is a strong
446 stimulus for oxidative stress as visible by the increase of MDA and of protein carbonylation (used as markers
447 of lipid peroxidation and protein damage secondary to oxidative stress, respectively) and by the reduction of
448 SOD activity. The amelioration of oxidative balance following *L*-Ctl treatment, further describes the peptide
449 as a novel candidate in the treatment of septic cardiomyopathy. Moreover, in line with our results, LPS-

450 induced oxidative stress may additionally contribute to the activation of NFκB that, in turn, may further
451 impact the cardiomyocytes inflammation that is finally mitigated/abolished by Ctl.

452 **5. Conclusions**

453 Taken together our results describe Ctl as a potential anti-inflammatory/anti-microbial therapeutic agent, and
454 its inhibition of TLR4 by targeting MD-2 could represent an effective tool to counteract sepsis and septic
455 shock induced by Gram negative bacteria in addition to its interesting and protective antioxidant properties.
456 These data are of interest considering that Ctl efficacy and resistance have been extensively demonstrated in
457 several microbial strains. Moreover, being a short and linear peptide, stable in a wide range of pH and
458 temperature, Ctl would be easily synthesized at a minimal cost making it an excellent candidate for future
459 drug development.

460 **Author Contributions**

461 The individual contributions of the authors are specified as follows: Conceptualization, Carmine Rocca and
462 Tommaso Angelone; Data curation, Carmine Rocca, Anna De Bartolo, Fedora Grande, Bruno Rizzuti,
463 Teresa Pasqua, Francesca Giordano, Maria Concetta Granieri, Maria Antonietta Occhiuzzi and Nicola
464 Amodio; Methodology, Carmine Rocca, Anna De Bartolo, Fedora Grande, Bruno Rizzuti, Teresa Pasqua,
465 Francesca Giordano, Maria Concetta Granieri, Maria Antonietta Occhiuzzi and Nicola Amodio; Supervision,
466 Marie-Hélène Metz-Boutigue and Tommaso Angelone; Validation, Carmine Rocca, Anna De Bartolo,
467 Fedora Grande, Bruno Rizzuti, Teresa Pasqua, Francesca Giordano, Maria Concetta Granieri, Maria
468 Antonietta Occhiuzzi, Nicola Amodio and Tommaso Angelone; Writing – original draft, Carmine Rocca,
469 Anna De Bartolo, Fedora Grande, Bruno Rizzuti, Teresa Pasqua and Tommaso Angelone; Writing – review
470 & editing, Antonio Garofalo, Nicola Amodio, Maria Carmela Cerra, Francis Schneider, Maria Luisa Panno
471 and Marie-Hélène Metz-Boutigue. All authors have read and approved the final version of the manuscript.

472 **Funding**

473 This work was supported by the Ministry of Education, University and Research (MIUR) of Italy (ex 60%),
474 Inserm UMR 1121 (France) and Doctorate School in “Life Science and Technology” (Italy).

475 **Acknowledgments**

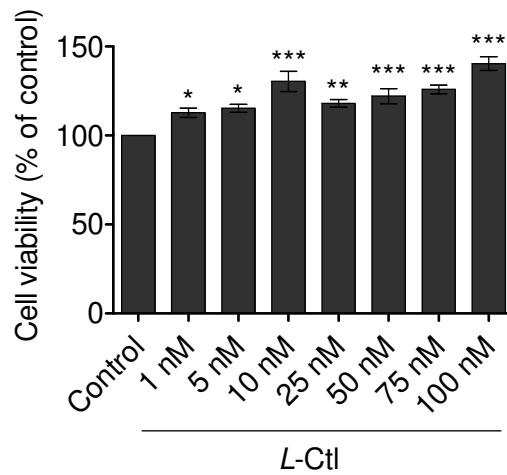
476 C.R. acknowledges POR Calabria (Italy) FESR-FSE 2014/2020-Azione 10.5.12-Linea B (DR n. 683 del
477 21/05/2019) for financial support for RTDa position. B.R. acknowledges the use of computational resources
478 from the European Magnetic Resonance Center (CERM), Sesto Fiorentino (Florence), Italy. T.P.
479 acknowledges PON “Ricerca e Innovazione” 2014–2020: AIM “Attraction and International Mobility”
480 (MIUR, Italy) for financial support for RTDa position.

481 **Conflicts of Interest**

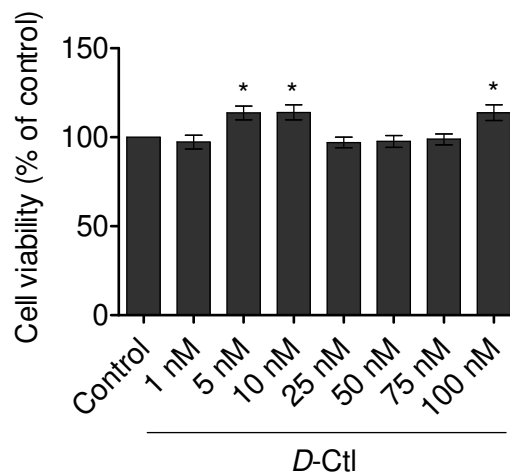
482 The authors declare no conflicts of interest.

483
484

A



B



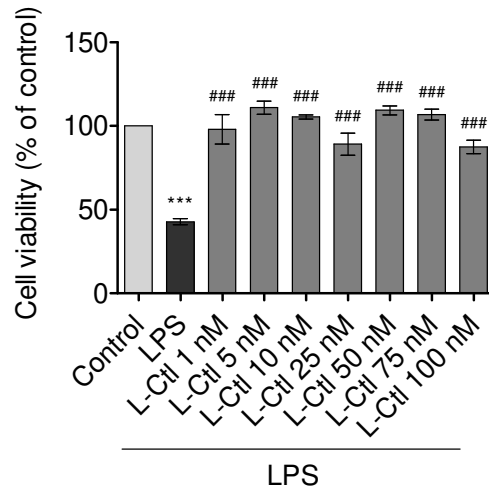
485
486

487 **Figure 1. Effects of *L*-cateslytin (*L*-Ctl) and *D*-cateslytin (*D*-Ctl) on cell viability in H9c2**
488 **cardiomyocytes.**

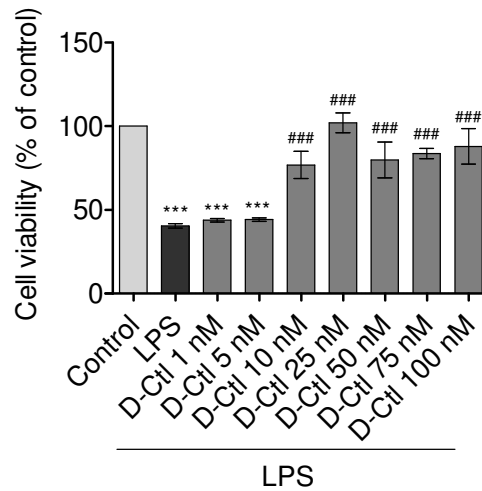
489 H9c2 cardiomyocytes were treated with vehicle (Control) or increasing concentration of **A**) *L*-Ctl (1-100
490 nM) or **B**) *D*-Ctl (1-100 nM) for 6 h. Cell viability was determined using MTT assay and was expressed as
491 the percentage of control cells only exposed to vehicle (indicated as Control). Results are represented as
492 mean \pm SEM (n=6 per group). Significant differences were detected by one-way ANOVA followed by
493 Dunnett's test, $p < 0.05$ (*); $p < 0.01$ (**) and $p < 0.001$ (***) vs Control group.

494
495

A



B



496
497

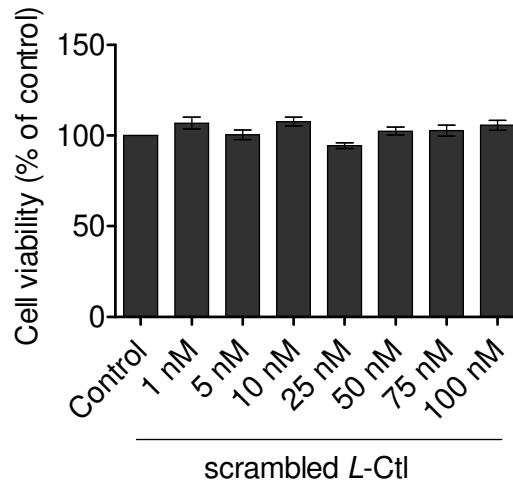
498 **Figure 2. Effects of *L*-Ctl and *D*-Ctl in the presence of lipopolysaccharide (LPS) on H9c2**
499 **cardiomyocytes viability.**

500 H9c2 cardiomyocytes were treated with vehicle (Control) or LPS (10 μ g/mL) alone and in co-treatment with
501 increasing concentration of **A)** *L*-Ctl (1-100 nM) or **B)** *D*-Ctl (1-100 nM) for 6 h. Cell viability was
502 determined using MTT assay and was expressed as the percentage of control cells only exposed to vehicle
503 (indicated as Control). Results are represented as mean \pm SEM (n=6 per group). Significant differences were

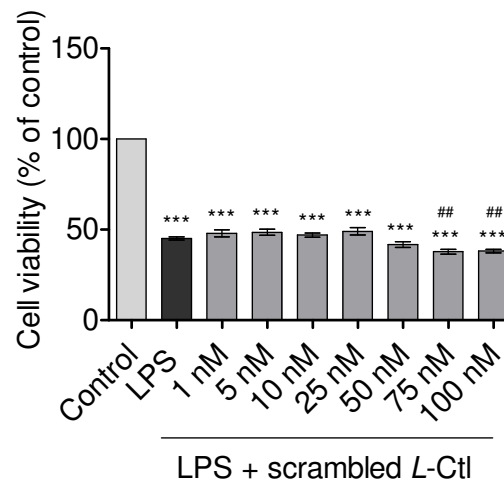
504 detected by one-way ANOVA and Newman-Keuls multiple comparison test. $p < 0.001$ (***) vs Control
505 group; $p < 0.001$ (###) vs LPS group.

506

A



B



507

508

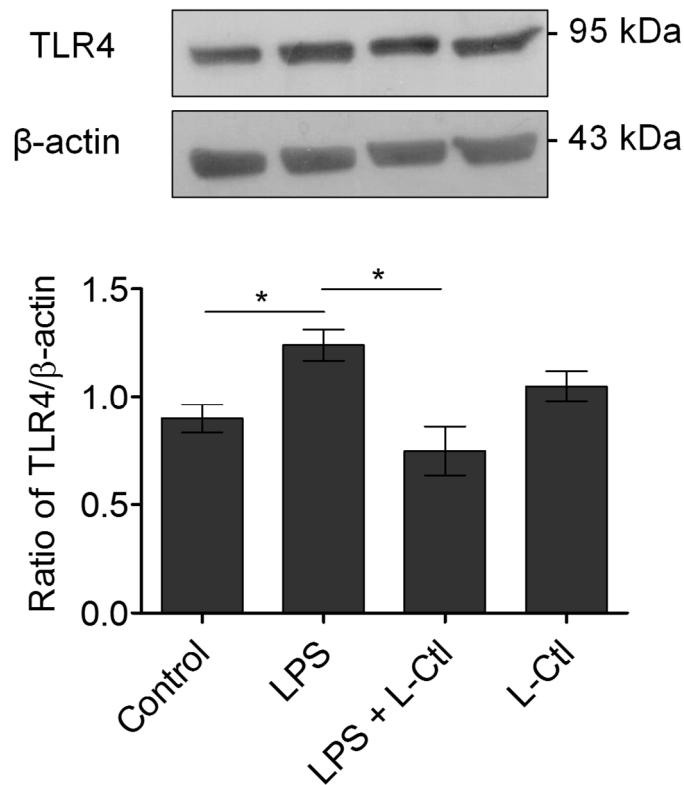
509 **Figure 3. Effect of scrambled L-Ctl in the absence or in the presence of LPS on H9c2 cardiomyocytes**
510 **viability**

511 H9c2 cardiomyocytes were treated with vehicle (Control) or increasing concentration of scrambled L-Ctl (1-
512 100 nM) for 6 h A) Cell viability was determined using MTT assay and was expressed as the percentage of
513 control cells only exposed to vehicle (indicated as Control). Results are represented as mean \pm SEM (n=6 per
514 group). Statistical analysis was carried out by one-way ANOVA followed by Dunnett's test.

515 H9c2 cardiomyocytes were treated with vehicle (Control) or LPS (10 $\mu\text{g}/\text{mL}$) alone and in co-treatment with
516 increasing concentration of scrambled *L*-Ctl (1-100 nM) for 6 h **B**) Significant differences were detected by
517 one-way ANOVA and Newman-Keuls multiple comparison test. $p < 0.001$ (***) vs Control group; $p < 0.01$
518 (##) vs LPS group.

519

520



521

522

523 **Figure 4. Influence of *L*-Ctl on toll like receptor 4 (TLR4) expression in H9c2 cardiomyocytes**
524 **stimulated with LPS.**

525 Western blot analysis of TLR4 in H9c2 cardiomyocytes exposed to vehicle (indicated as Control), LPS (10
526 $\mu\text{g}/\text{mL}$), LPS + *L*-Ctl (1 nM) (n=3 independent experiments) [mouse monoclonal antibody against TLR4
527 (Cat# sc-293072, RRID:AB_10611320) and β -actin (Cat# sc-69879, RRID:AB_1119529) Santa Cruz
528 Biotechnology (Dallas, Texas, USA)]. Histograms represent the ratio of densitometric analysis of
529 protein:loading control. Significant differences were detected by one-way ANOVA and Newman-Keuls
530 multiple comparison test. $p < 0.05$ (*).

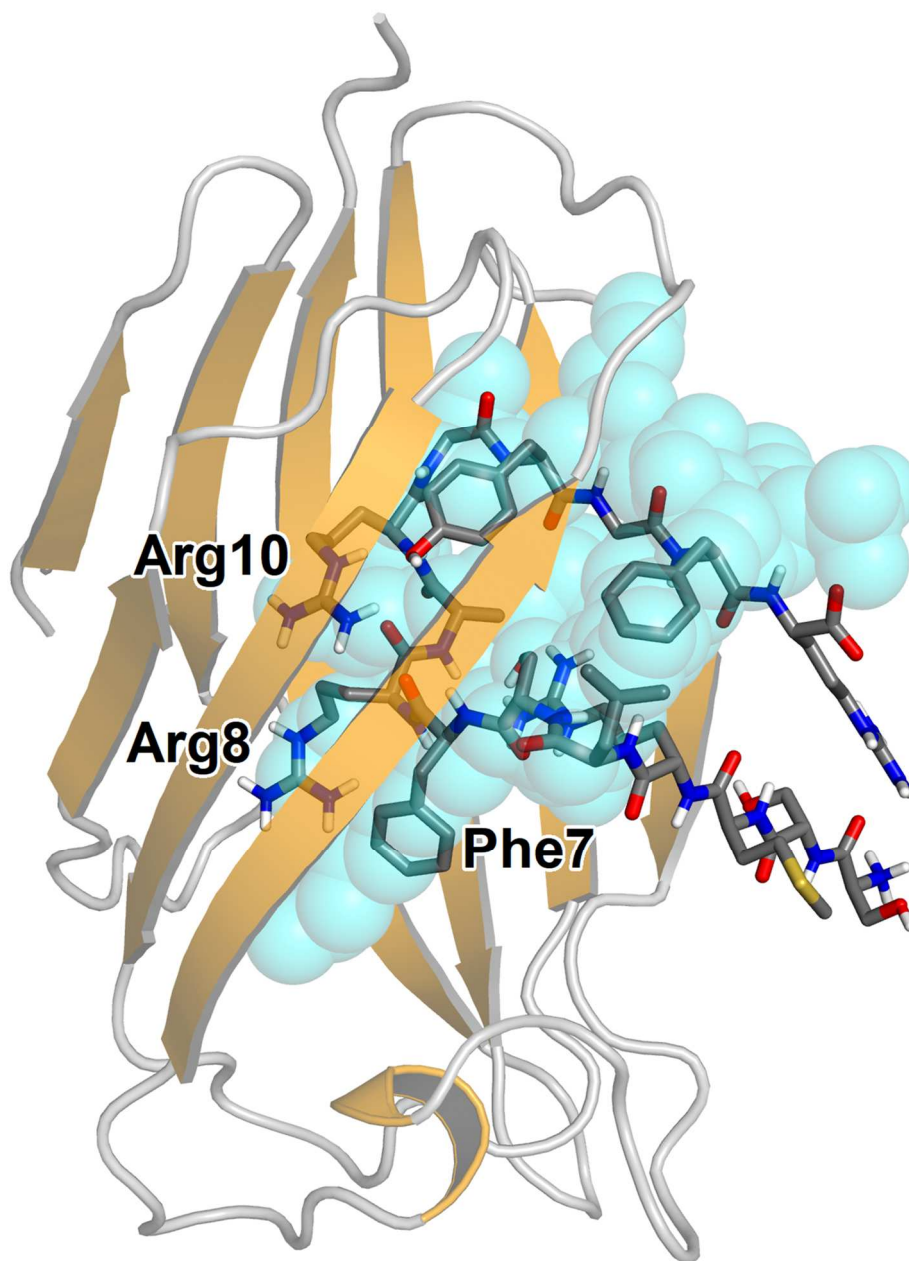
531

532

533

534

535
536
537
538
539



540
541
542
543
544
545
546
547

Figure 5. Binding of Ctl to myeloid differentiation factor 2 (MD-2).

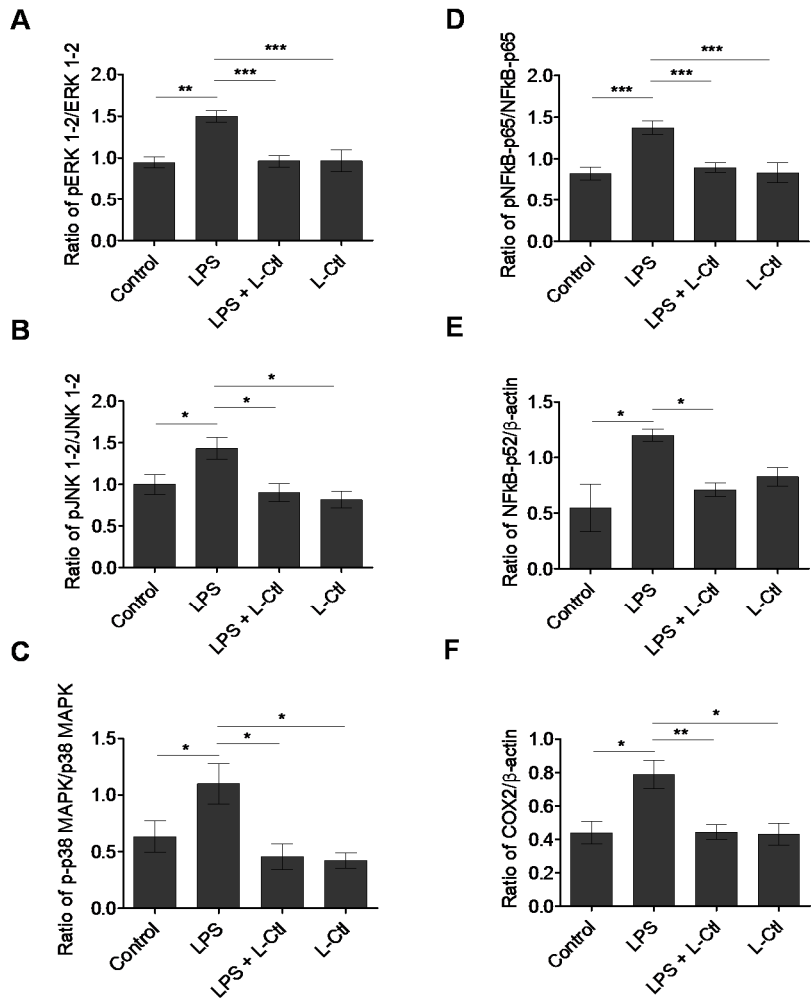
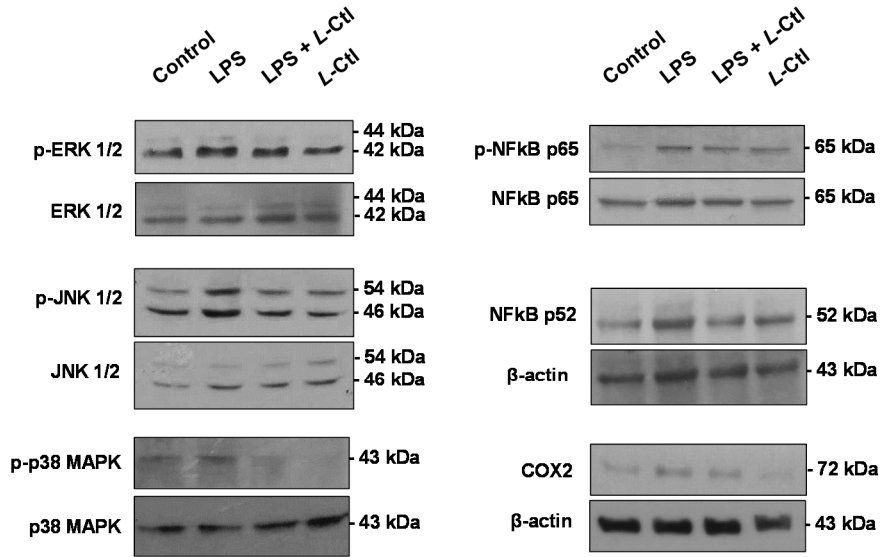
Most favorable structure of Ctl (stick representation, with colored atoms) bound in the binding site of MD-2 (yellow cartoon representation), superimposed to the volume occupied in the same pocket by physiological ligands (cyan spheres) in the crystallographic structure of the protein [34]. Image created with PyMol [69].

548

549

550

551



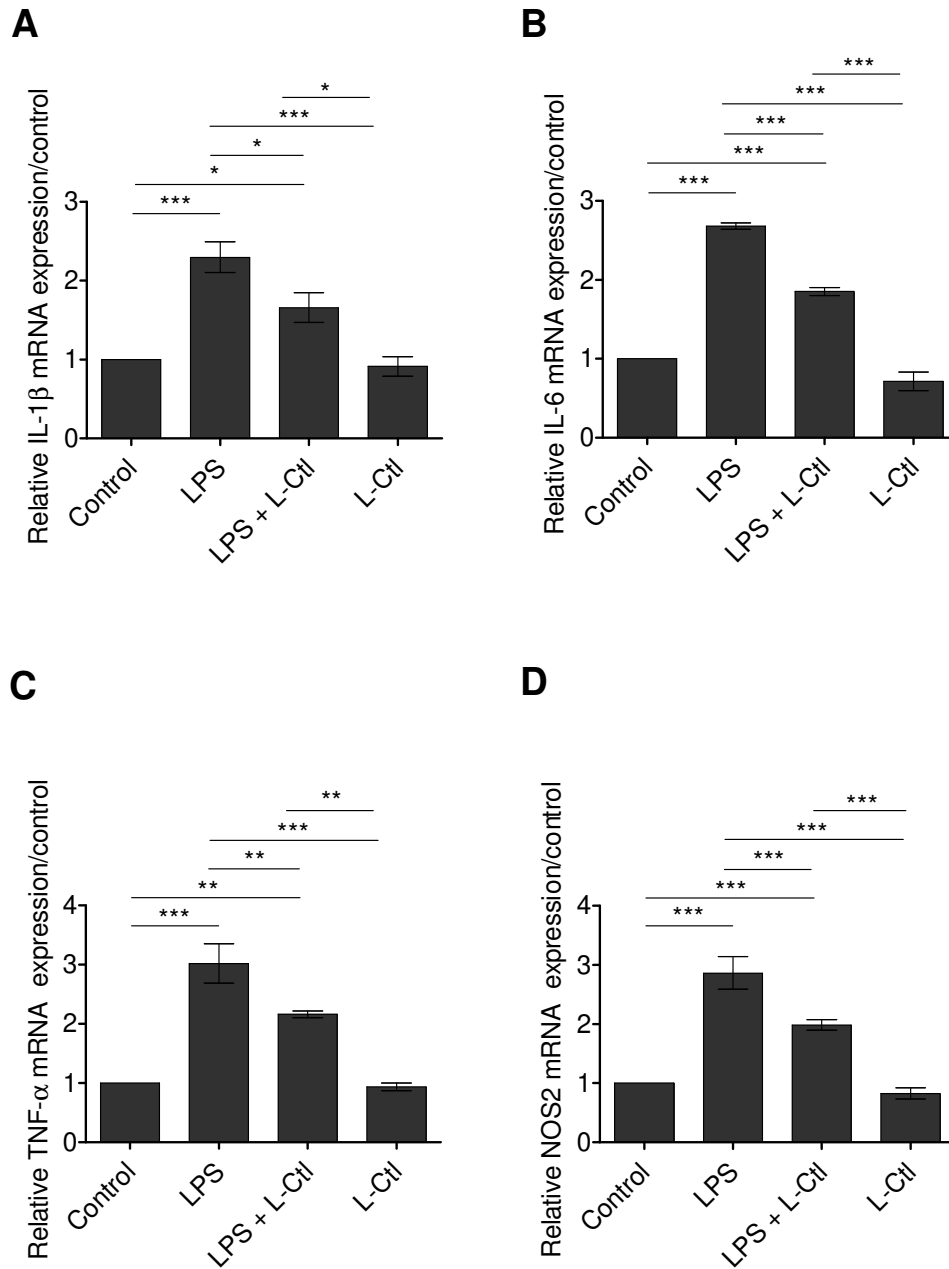
552

553
554
555
556
557
558
559
560
561
562
563
564
565
566
567
568
569
570
571
572
573
574
575
576
577
578
579
580
581
582
583

Figure 6. Molecular mechanism activated by *L*-Ctl in H9c2 cardiomyocytes.

Western blot analysis of **A) phospho- extracellular-signal-regulated kinase 1/2 (p-ERK1/2), B) phospho-c-JunN-terminal kinase 1/2 (p-JNK1/2), C) phospho-p38 mitogen-activated protein kinase (p38 MAPK), D) nuclear factor kappa-light-chain-enhancer of activated B cells (NFkB) p65 (p-NFkB p65), E) NFkB p52 and F) cyclooxygenase-2 (COX2)** in H9c2 cardiomyocytes exposed to vehicle (indicated as Control), LPS (10 μ g/mL), LPS + *L*-Ctl (1 nM) and *L*-Ctl (1 nM) (n=3 independent experiments) for 6 h [mouse monoclonal antibodies against **p-ERK1/2 (Cat# sc-7383), ERK1/2 (Cat# sc-514302), NFkB p65 (Cat# sc-8008), NFkB p52 (Cat# sc-7386, RRID:AB_2267131) Santa Cruz Biotechnology (Dallas, Texas, USA), p-NFkB p65 (#13346), Cell Signaling Technology, Inc, (Danvers, Massachusetts, USA),** or rabbit polyclonal antibodies against **p-SAPK/JNK (#9251), SAPK/JNK (#9252), p-p38 MAPK (#9211) or p38 MAPK (#9218), Cell Signaling Technology, or COX2 (Cat# TA313292), OriGene Technologies (Rockville, Maryland, USA)].** Histograms represent the ratio of densitometric analysis of protein:loading control. Significant differences were detected by one-way ANOVA and Newman-Keuls multiple comparison test. $p < 0.05$ (*); $p < 0.01$ (**); $p < 0.001$ (***)].

584
585
586
587
588



589
590
591
592

Figure 7. Effects of L-Ctl on the LPS-induced mRNA expression of inflammatory mediators in H9c2 cells.

593 Evaluation of mRNA expression levels of **A**) interleukin (IL)-1 β , **B**) IL-6, **C**) tumor necrosis factor (TNF)- α ,
594 and **D**) nitric oxide synthase (NOS) 2 (inducible) by quantitative reverse-transcription real-time PCR (qRT-
595 PCR) in H9c2 cardiomyocytes exposed to vehicle (indicated as Control), LPS (10 μ g/mL), LPS + L-Ctl (1
596 nM) and L-Ctl (1 nM) for 6 h. Samples were analyzed in triplicate, the relative mRNA expression levels of
597 the different genes were normalized to rRNA18S and calculated on the basis of the $2^{-\Delta\Delta C_t}$ method. Data are
598 expressed as the mean \pm SEM of 3 separate experiments. Significant differences were detected by one-way
599 ANOVA and Newman-Keuls multiple comparison test. $p < 0.05$ (*); $p < 0.01$ (**); $p < 0.001$ (***)).

600

601

602

603

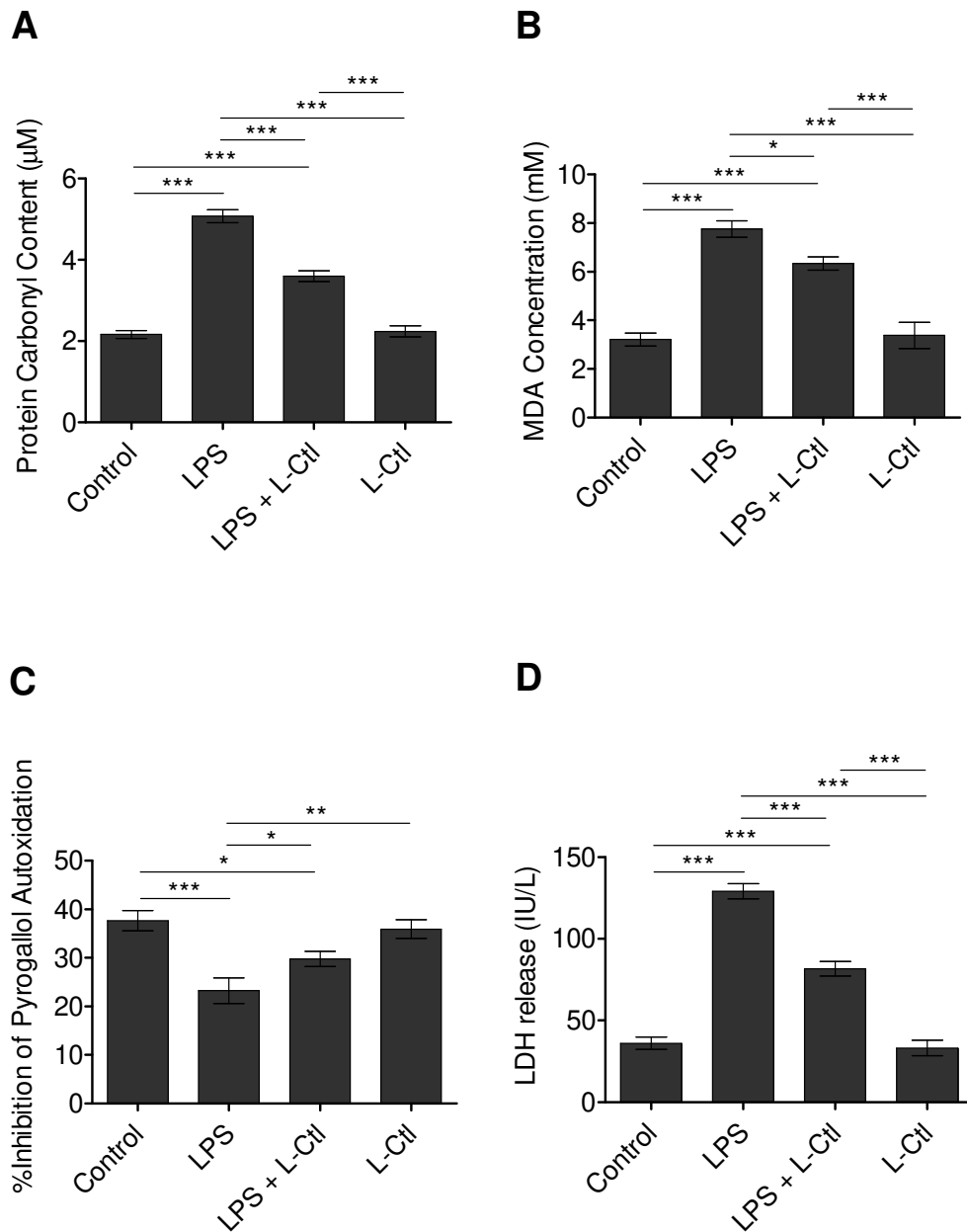
604

605

606

607

608



609

610

611 **Figure 8. Effect of *L*-Ctl on malondialdehyde (MDA) levels, protein carbonyl groups content,**
 612 **superoxide dismutase (SOD) activity and lactate dehydrogenase (LDH) release in LPS-treated H9c2**
 613 **cells.**

614 MDA concentration **A**), protein carbonyl groups content **B**) and SOD activity **C**) in lysates of H9c2
 615 cardiomyocytes treated with vehicle (Control), LPS (10 µg/mL), LPS + *L*-Ctl (1 nM) and *L*-Ctl (1 nM) for 6
 616 h. MDA concentration was expressed as mmol/L, protein carbonyl groups content was expressed as µmol/L
 617 and SOD activity was expressed as percentage of inhibition of the pyrogallol autoxidation rate. Data are
 618 expressed as the mean ± SEM of six separate experiments. Significant differences were detected by one-way
 619 ANOVA and Newman-Keuls multiple comparison test. $p < 0.05$ (*); $p < 0.01$ (**); $p < 0.001$ (***)

620 release in the supernatant of H9c2 cardiomyocytes treated with vehicle (Control), LPS (10 µg/mL), LPS + L-
621 Ctl (1 nM) and L-Ctl (1 nM) for 24 h **D**). The result of LDH activity was expressed as IU/L. Data are
622 expressed as the mean ± SEM of six separate experiments. Significant differences were detected by one-way
623 ANOVA and Newman-Keuls multiple comparison test. $p < 0.001$ (***).

624

625 **References**

- 626 [1] S.P. Caforio, E. Arbustini, C. Basso, J. Gimeno-Blanes, S.B. Felix, M. Fu, T. Heliö, S. Heymans, R.
627 Jahns, K. Klingel, A. Linhart, B. Maisch, W. McKenna, J. Mogensen, Y.M. Pinto, A. Ristic, H.P.
628 Schultheiss, H. Seggewiss, L. Tavazzi, G. Thiene, A. Yilmaz, P. Charron, P.M. Elliott, Current state
629 of knowledge on aetiology, diagnosis, management, and therapy of myocarditis: a position statement
630 of the European Society of Cardiology Working Group on Myocardial and Pericardial Diseases. *Eur.*
631 *Heart J.* (2013), 2636-48. <https://doi.org/10.1093/eurheartj/ehf210>.
- 632 [2] V.O. Puntmann, M.L. Carerj, I. Wieters, M. Fahim, C. Arendt, J. Hoffmann, A. Shchendrygina, F.
633 Escher, M. Vasa-Nicotera, A.M. Zeiher, M. Vehreschild, E. Nagel, 2020. Outcomes of
634 Cardiovascular Magnetic Resonance Imaging in Patients Recently Recovered From Coronavirus
635 Disease 2019 (COVID-19). *JAMA Cardiol.*, e203557.
636 <https://doi.org/10.1001/jamacardio.2020.3557>.
- 637 [3] F. Moccia, A. Gerbino, V. Lionetti, M. Miragoli, L.M. Munaron, P. Pagliaro, T. Pasqua, C. Penna,
638 C. Rocca, M. Samaja, T. Angelone, COVID-19-associated cardiovascular morbidity in older adults:
639 a position paper from the Italian Society of Cardiovascular Researches. *Geroscience* (2020), 1-29.
640 <https://doi.org/10.1007/s11357-020-00198-w>.
- 641 [4] A. Vieillard-Baron, V. Caille, C. Charron, G. Belliard, B. Page, F. Jardin, Actual incidence of global
642 left ventricular hypokinesia in adult septic shock. *Crit. Care Med.* (2008), 1701-1706.
643 <https://doi.org/10.1097/ccm.0b013e318174db05>.
- 644 [5] M.W. Merx, C. Weber, Sepsis and the heart. *Circulation* (2007), 793-802.
645 <https://doi.org/10.1161/CIRCULATIONAHA.106.678359>.
- 646 [6] S. Frantz, L. Kobzik, Y.D. Kim, R. Fukazawa, R. Medzhitov, R.T. Lee, R.A. Kelly, Toll4 (TLR4)
647 expression in cardiac myocytes in normal and failing myocardium. *J. Clin. Invest.* (1999), 271-280.
648 <https://doi.org/10.1172/JCI6709>.
- 649 [7] Y. Yang, J. Lv, S. Jiang, Z. Ma, D. Wang, W. Hu, C. Deng, C. Fan, S. Di, Y. Sun, W. Yi, 2016. The
650 emerging role of Toll-like receptor 4 in myocardial inflammation. *Cell Death Dis.*, 7(5): e2234.
651 <https://doi.org/10.1038/cddis.2016.140e>.
- 652 [8] R.N. Naylor, R. Atun, N. Zhu, K. Kulasabanathan, S. Silva, A. Chatterjee, G.M. Knight, J.V.
653 Robotham, Estimating the burden of antimicrobial resistance: a systematic literature review.
654 *Antimicrob. Resist. Infect. Control.* (2018), 7: 58. <https://doi.org/10.1186/s13756-018-0336-y>.

- 655 [9] M. Mateescu, S. Baixe, T. Garnier, L. Jierry, V. Ball, Y. Haikel, M.H. Metz-Boutigue, M. Nardin, P.
656 Schaaf, O. Etienne, P. Lavalley, 2015. Antibacterial Peptide- Based Gel for Prevention of Medical
657 Implanted-Device Infection. PLoS One, 10(12), e0145143.
658 <https://doi.org/10.1371/journal.pone.0145143>.
- 659 [10] D. Zhang, P. Shooshtarizadeh, B.J. Laventie, D.A. Colin, J.F. Chich, J. Vidic, J. de Barry, S.
660 Chasserot-Golaz, F. Delalande, A. Van Dorsselaer, F. Schneider, K. Helle, D. Aunis, G. Prévost,
661 M.H. Metz-Boutigue, 2009. Two Chromogranin A-Derived Peptides Induce Calcium Entry in
662 Human Neutrophils by Calmodulin-Regulated Calcium Independent Phospholipase A2. PLoS One,
663 4(2), e4501. <https://doi.org/10.1371/journal.pone.0004501>.
- 664 [11] E. Glattard, T. Angelone, J.M. Strub, A. Corti, D. Aunis, B. Tota, M.H. Metz-Boutigue, Y.
665 Goumon, Characterization of natural vasostatin-containing peptides in rat heart. FEBS J. (2006),
666 3311-3321. <https://doi.org/10.1111/j.1742-4658.2006.05334.x>.
- 667 [12] K.B. Helle, M.H. Metz-Boutigue, M.C. Cerra, T. Angelone, Chromogranins: from discovery to
668 current times. Pflugers Arch (2018), 143-154. <https://doi.org/10.1007/s00424-017-2027-6>.
- 669 [13] T. Pasqua, C. Rocca, A. Spena, T. Angelone, M.C. Cerra, Modulation of the coronary tone in the
670 expanding scenario of Chromogranin-A and its derived peptides. Future Med. Chem., Volume 11,
671 Issue 12, 2019, Pages 1501-1511.
- 672 [14] T. Pasqua, A. Corti, S. Gentile, L. Pochini, M. Bianco, M.H. Metz-Boutigue, M.C. Cerra, B. Tota,
673 T. Angelone, Full-length human chromogranin-A cardioactivity: myocardial, coronary, and
674 stimulus-induced processing evidence in normotensive and hypertensive male rat hearts.
675 Endocrinology (2013), 154(9):3353-65. <https://doi.org/10.1210/en.2012-2210>.
- 676 [15] J. Troger, M. Theurl, R. Kirchmair, T. Pasqua, B. Tota, T. Angelone, M.C. Cerra, Y. Nowosielski,
677 R. Mätzler, J. Troger, J.R. Gayen, V. Trudeau, A. Corti, K.B. Helle, Granin-derived peptides. Prog
678 Neurobiol. (2017), 154:37-61. <https://doi.org/10.1016/j.pneurobio.2017.04.003>.
- 679 [16] L. Taupenot, S.K. Mahata, M. Mahata, R.J. Parmer, D.T. O'Connor, Interaction of the
680 catecholamine release-inhibitory peptide catestatin (human chromogranin A (352-372)) with the
681 chromaffin cell surface and Torpedo electroplax: implications for nicotinic cholinergic antagonism.
682 Regul. Pept. (2000), 9-17. [https://doi.org/10.1016/s0167-0115\(00\)00135-x](https://doi.org/10.1016/s0167-0115(00)00135-x).
- 683 [17] E.M. Muntjewerff, G. Dunkel, M.J.T. Nicolassen, S.K. Mahata, G. van den Bogaart, Catestatin as a
684 Target for Treatment of Inflammatory Diseases. Front. Immunol. (2018), 9: 2199.
685 <https://doi.org/10.3389/fimmu.2018.02199>.
- 686 [18] P. Darteville, C. Ehlinger, A. Zaet, C. Boehler, M. Rabineau, B. Westermann, J.M. Strub, S.
687 Cianferani, Y. Haikel, M.H. Metz-Boutigue, C. Marban, D-Cateslytin: a new antifungal agent for the
688 treatment of oral *Candida albicans* associated infections. Sci. Rep. (2018), 18; 9235.
689 <https://doi.org/10.1038/s41598-018-27417-x>.

- 690 [19] R. Aslam, M. Atindehou, T. Lavaux, Y. Haïkel, F. Schneider, M.H. Metz-Boutigue, Chromogranin
691 A-derived peptides are involved in innate immunity. *Curr. Med. Chem.* (2012), 4115-4123.
692 <https://doi.org/10.2174/092986712802430063>.
- 693 [20] A. Zaet, P. Dartevelle, F. Daouad, C. Ehlinger, F. Quilès, G. Francius, C. Boehler, C. Bergthold, B.
694 Frisch, G. Prévost, P. Lavalley, F. Schneider, Y. Haïkel, M.H. Metz-Boutigue, C. Marban, D-
695 Cateslytin, a new antimicrobial peptide with therapeutic potential. *Sci. Rep.* (2017), 15199.
696 <https://doi.org/10.1038/s41598-017-15436-z>.
- 697 [21] C. Rocca, S. Femminò, G. Aquila, M.C. Granieri, E.M. De Francesco, T. Pasqua, D.C. Rigracciolo,
698 F. Fortini, M.C. Cerra, M. Maggiolini, P. Pagliaro, P. Rizzo, T. Angelone, C. Penna, Notch1
699 Mediates Preconditioning Protection Induced by GPER in Normotensive and Hypertensive Female
700 Rat Hearts. *Front. Physiol.* (2018), 9-521. <https://doi.org/10.3389/fphys.2018.00521>.
- 701 [22] Y. Zheng, S. Li, R. Hu, F. Cheng, L. Zhang, GFI-1 Protects Against Lipopolysaccharide-Induced
702 Inflammatory Responses and Apoptosis by Inhibition of the NF- κ B/TNF- α Pathway in H9c2 Cells.
703 *Inflammation* (2020), 74-84. <https://doi.org/10.1007/s10753-019-01095-x>.
- 704 [23] M.J. McQueen, Optimal Assay of LDH and α -HBD at 37 °C. *Ann. Clin. Biochem.* (1972), 9, 2.
705 <https://doi.org/10.1177/000456327200900102>.
- 706 [24] C. Rocca, F. Scavello, B. Colombo, A.M. Gasparri, A. Dallatomasina, M.C. Granieri, D. Amelio, T.
707 Pasqua, M.C. Cerra, B. Tota, A. Corti, T. Angelone, Physiological levels of chromogranin A prevent
708 doxorubicin-induced cardiotoxicity without impairing its anticancer activity. *FASEB J.* (2019),
709 7734-7747. <https://doi.org/10.1096/fj.201802707R>.
- 710 [25] S.F. Assimakopoulos, C.E. Vagianos, G. Zervoudakis, K.S. Filos, C. Georgiou, V. Nikolopoulou,
711 C.D. Scopa, Gut regulatory peptides bombesin and neurotensin reduce hepatic oxidative stress and
712 histological alterations in bile duct ligated rats. *Regul. Pept.* (2004), 185– 193.
713 <https://doi.org/10.1016/j.regpep.2004.03.010>.
- 714 [26] M.R. Preetha Rani, N. Anupama, M. Sreelekshmi, K.G. Raghu, Chlorogenic acid attenuates
715 glucotoxicity in H9c2 cells via inhibition of glycation and PKC α upregulation and safeguarding
716 innate antioxidant status. *Biomed. Pharmacother.* (2018), 467-4777.
717 <https://doi.org/10.1016/j.biopha.2018.02.027>.
- 718 [27] T. Pasqua, C. Rocca, F. R. Lupi, N. Baldino, D. Amelio, O. I. Parisi, M. C. Granieri, A. De Bartolo,
719 A. Lauria, M. Dattilo, I. D. Perrotta, F. Puoci, M. C. Cerra, D. Gabriele, T. Angelone, Cardiac and
720 Metabolic Impact of Functional Foods with Antioxidant Properties Based on Whey Derived Proteins
721 Enriched with Hemp Seed Oil. *Antioxidants* (2020), 9 (11) 1066.
722 <https://doi.org/10.3390/antiox9111066>.
- 723 [28] A.Z. Reznick, L. Packer, Oxidative damage to proteins: spectrophotometric method for carbonyl
724 assay. *Methods Enzymol.* (1994), 357-63. [https://doi.org/10.1016/s0076-6879\(94\)33041-7](https://doi.org/10.1016/s0076-6879(94)33041-7).

- 725 [29] S. Marklund, G. Marklund, Involvement of the superoxide anion radical in the autoxidation of
726 pyrogallol and a convenient assay for superoxide dismutase. *Eur. J. Biochem.* (1974), 469-74.
727 <https://doi.org/10.1111/j.1432-1033.1974.tb03714.x>.
- 728 [30] A. Thakur, J. Alam M.R. Ajayakumar, S. Ghaskadbi, M. Sharma, S.K. Goswami, Norepinephrine-
729 induced apoptotic and hypertrophic responses in H9c2 cardiac myoblasts are characterized by
730 different repertoire of reactive oxygen species generation. *Redox Biology* (2015), 243-252.
731 <https://doi.org/10.1016/j.redox.2015.05.005>.
- 732 [31] C. Rocca, L. Boukhzar, M.C. Granieri, I. Alsharif, R. Mazza, B. Lefranc, B. Tota, J. Leprince, M.C.
733 Cerra, Y. Anouar, T Angelone, 2018. A selenoprotein T-derived peptide protects the heart against
734 ischaemia/reperfusion injury through inhibition of apoptosis and oxidative stress. *Acta Physiol.*,
735 223(4):e13067. <https://doi.org/10.1111/apha.13067>.
- 736 [32] C. Rocca, F. Scavello, M.C. Granieri, T. Pasqua, N. Amodio, S. Imbrogno, A. Gattuso, R. Mazza,
737 M.C. Cerra, T. Angelone, Phoenixin-14: detection and novel physiological implications in cardiac
738 modulation and cardioprotection. *Cell. Mol. Life Sci.* (2018), 743-756.
739 <https://doi.org/10.1007/s00018-017-2661-3>.
- 740 [33] O. Trott, A.J. Olson, AutoDock Vina: Improving the speed and accuracy of docking with a new
741 scoring function, efficient optimization, and multithreading. *J. Comput. Chem.* (2010), 455-461.
742 <https://doi.org/10.1002/jcc.21334>.
- 743 [34] U. Ohto, N. Yamakawa, S. Akashi-Takamura, K. Miyake, T. Shimizu, Structural analyses of human
744 Toll-like receptor 4 polymorphisms D299G and T399I. *J. Biol. Chem.* (2012), 40611-40617.
745 <https://doi.org/10.1074/jbc.M112.404608>.
- 746 [35] E.F. Pettersen, T.D. Goddard, C.C. Huang, G.S. Couch, D.M. Greenblatt, E.C. Meng, T.E. Ferrin,
747 UCSF Chimera - A visualization system for exploratory research and analysis. *J. Comput. Chem.*
748 (2004), 1605–1612. <https://doi.org/10.1002/jcc.20084>.
- 749 [36] P. Santofimia-Castaño, B. Rizzuti, Á.L. Pey, P. Soubeyran, M. Vidal, R. Urrutia, J.L. Iovanna, J.L.
750 Neira, Intrinsically disordered chromatin protein NUPR1 binds to the C-terminal region of Polycomb
751 RING1B. *PNAS* (2017), 6332-6341. <https://doi.org/10.1073/pnas.1619932114>.
- 752 [37] R. Lappano, C. Mallet, B. Rizzuti, F. Grande, G.R. Galli, C. Byrne, I. Broutin, L. Boudieu, A.
753 Eschalier, Y. Jacquot, M. Maggiolini, The Peptide ER α 17p Is a GPER Inverse Agonist that Exerts
754 Antiproliferative Effects in Breast Cancer Cells. *Cells* (2019), 590.
755 <https://doi.org/10.3390/cells8060590>.
- 756 [38] M. Sugawara, J.M. Resende, C. Mendonca de Moraes, J.F. Chich, A. Marquette, M.H. Metz-
757 Boutigue, B. Bechinger, Membrane structure and interactions of human Catestatin by
758 multidimensional solution and solid-state NMR spectroscopy. *FASEB J.* (2010), 1737-1746.
759 <https://doi.org/10.1096/fj.09-142554>.

- 760 [39] F. Grande, B. Rizzuti, M.A. Occhiuzzi, G. Ioele, T. Casacchia, F. Gelmini, R. Guzzi, A. Garofalo,
761 G. Statti, Identification by molecular docking of homoisoflavones from *Leopoldia comosa* as ligands
762 of estrogen receptors. *Molecules* (2018), 23, 894. <https://doi.org/10.3390/molecules23040894>.
- 763 [40] T. Casacchia, M.A. Occhiuzzi, F. Grande, B. Rizzuti, M.C. Granieri, C. Rocca, A. Gattuso, A.
764 Garofalo, T. Angelone, G. Statti, A pilot study on the nutraceutical properties of the Citrus hybrid
765 Tacle® a dietary source of polyphenols for supplementation in metabolic disorders. *J. Funct. Foods*
766 (2019), 370-381. <https://doi.org/10.1016/j.jff.2018.11.030>.
- 767 [41] T. Angelone, E. Filice, A.M. Quintieri, S. Imbrogno, N. Amodio, T. Pasqua, D. Pellegrino, F. Mulè,
768 M.C. Cerra, Receptor identification and physiological characterisation of glucagon-like peptide-2 in
769 the rat heart. *Nutr. Metab. Cardiovasc. Dis.* (2012), 486-94.
770 <https://doi.org/10.1016/j.numecd.2010.07.014>.
- 771 [42] I.C. Nettore, C. Rocca, G. Mancino, L. Albano, D. Amelio, F. Grande, F. Puoci, T. Pasqua, S.
772 Desiderio, R. Mazza, D. Terracciano, A. Colao, F. Bèguinot, G.L. Russo, M. Dentice, P.E. Macchia,
773 M.S. Sinicropi, T. Angelone, P. Ungaro, Quercetin and its derivative Q2 modulate chromatin
774 dynamics in adipogenesis and Q2 prevents obesity and metabolic disorders in rats. *J. Nutr. Biochem.*
775 (2019), 69:151-162. <https://doi.org/10.1016/j.jnutbio.2019.03.019>.
- 776 [43] Y. Wang, L. Su, M.D. Morin, B.T. Jones, L.R. Whitby, M.M.R.P. Surakattula, H. Huang, H. Shi,
777 J.H. Choi, K. Wang, E.M.Y. Moresco, M. Berger, X. Zhan, H. Zhang, D.L. Boger, B. Beutler,
778 TLR4/MD-2 activation by a synthetic agonist with no similarity to LPS. *PNAS* (2016), 884-893.
779 <https://doi.org/10.1073/pnas.1525639113>.
- 780 [44] Z. Golkar, O. Bagasra, D.G. Pace, Bacteriophage therapy: a potential solution for the antibiotic
781 resistance crisis. *J. Infect. Dev. Ctries.* (2014), 129-136. <https://doi.org/10.3855/jidc.3573>.
- 782 [45] M. Mahlapuu, J. Håkansson, L. Ringstad, C. Björn, Antimicrobial Peptides: An Emerging Category
783 of Therapeutic Agents. *Front. Cell. Infect. Microbiol.* (2016), 6, 194.
784 <https://doi.org/10.3389/fcimb.2016.00194>.
- 785 [46] R.E. Hancock, H.G. Sahl, Antimicrobial and host-defense peptides as new anti-infective therapeutic
786 strategies. *Nat. Biotechnol.* (2006), 1551–1557. <https://doi.org/10.1038/nbt1267>.
- 787 [47] M.R. Yeaman, N.Y. Yount, Mechanisms of antimicrobial peptide action and resistance. *Pharmacol.*
788 *Rev.* (2003), 27-55. <https://doi.org/10.1124/pr.55.1.2>.
- 789 [48] M.H. Metz-Boutigue, A.E. Kieffer, Y. Goumon, D. Aunis, Innate immunity: involvement of new
790 neuropeptides. *Trends Microbiol.* (2003), 585-92. <https://doi.org/10.1016/j.tim.2003.10.001>.
- 791 [49] Q. Su, J. Yao, C. Sheng, Geniposide Attenuates LPS-Induced Injury via Up-Regulation of miR-145
792 in H9c2 Cells. *Inflammation* (2018), 1229–1237. <https://doi.org/10.1007/s10753-018-0769-8>.
- 793 [50] R. Wang, D. Li, J. Ouyang, X. Tian, Y. Zhao, X. Peng, S. Li, G. Yu, J. Yang, Leonurine alleviates
794 LPS-induced myocarditis through suppressing the NF- κ B signaling pathway. *Toxicology* (2019),
795 422:1-13. <https://doi.org/10.1016/j.tox.2019.04.011>.

- 796 [51] T.H. Htwe, N.M. Khardori, Cardiac emergencies: infective endocarditis, pericarditis, and
797 myocarditis. *Med. Clin. North Am.* (2012), 1149-69. <https://doi.org/10.1016/j.mcna.2012.09.003>.
- 798 [52] R. Hao, G. Su, X. Sun, X. Kong, C. Zhu 2, G. Su, Adiponectin attenuates lipopolysaccharide-
799 induced cell injury of H9c2 cells by regulating AMPK pathway. *Acta Biochim Biophys Sin*
800 (Shanghai) (2019), 51(2):168-177. doi: 10.1093/abbs/gmy162.
- 801 [53] N.H. Evans, Chiral Catenanes and Rotaxanes: Fundamentals and Emerging Applications. *Chemistry*
802 (2018), 3101-3112. <https://doi.org/10.1002/chem.201704149>.
- 803 [54] L. Chen, W. Fu, L. Zheng, Y. Wang, G. Liang, Recent progress in the discovery of myeloid
804 differentiation 2 (MD2) modulators for inflammatory diseases. *Drug Discov. today* (2018), 1187-
805 1202. <https://doi.org/10.1016/j.drudis.2018.01.015>.
- 806 [55] Y. Nagai, S. Akashi, M. Nagafuku, M. Ogata, Y. Iwakura, S. Akira, T. Kitamura, A. Kosugi, M.
807 Kimoto, K. Miyake, Essential role of MD-2 in LPS responsiveness and TLR4 distribution. *Nat.*
808 *Immunol.* (2002), 667-672. <https://doi.org/10.1038/ni809>.
- 809 [56] Y.C. Lu, W.C. Yeh, P.S. Ohashi, LPS/TLR4 signal transduction pathway. *Cytokine* (2008), 145-
810 151. <https://doi.org/10.1016/j.cyto.2008.01.006>.
- 811 [57] J.L. Lai, Y.H. Liu, C. Liu, M.P. Qi, R.N. Liu, X.F. Zhu, Q.G. Zhou, Y.Y. Chen, A.Z. Guo, C.M.
812 Hu, Indirubin Inhibits LPS-Induced Inflammation via TLR4 Abrogation Mediated by the NF- κ B and
813 MAPK Signaling Pathways. *Inflammation* (2017), (1):1-12. [https://doi.org/10.1007/s10753-016-](https://doi.org/10.1007/s10753-016-0447-7)
814 [0447-7](https://doi.org/10.1007/s10753-016-0447-7).
- 815 [58] Y.J. Choi, W.S. Lee, E.G. Lee, M.S. Sung, W.H. Yoo, Sulforaphane inhibits IL-1 β -induced
816 proliferation of rheumatoid arthritis synovial fibroblasts and the production of MMPs, COX-2, and
817 PGE2. *Inflammation* (2014), 1496-503. <https://doi.org/10.1007/s10753-014-9875-4>.
- 818 [59] B. Hoesel, J.A. Schmid, The complexity of NF- κ B signaling in inflammation and cancer. *Mol.*
819 *Cancer* (2013), 12, 86. <https://doi.org/10.1186/1476-4598-12-86>.
- 820 [60] A. Valaperti, Drugs targeting the canonical NF- κ B pathway to treat viral and autoimmune
821 myocarditis. *Curr. Pharm. Des.* (2016), 440-449.
822 <https://doi.org/10.2174/1381612822666151222160409>.
- 823 [61] T. Yu, D. Dong, J. Guan, J. Sun, M. Guo, Q. Wang, Alprostadil attenuates LPS-induced
824 cardiomyocyte injury by inhibiting the Wnt5a/JNK/NF- κ B pathway. *Herz* (2020), (Suppl
825 1):130-138. <https://doi.org/10.1007/s00059-019-4837-0>.
- 826 [62] C. Huang, Y. Zhang, H. Qi, X. Xu, L. Yang, J. Wang, Myc is involved in Genistein protecting
827 against LPS-induced myocarditis in vitro through mediating MAPK/JNK signaling pathway. *Biosci*
828 *Rep* (2020), 40(6):BSR20194472. <https://doi.org/10.1042/BSR20194472>.
- 829 [63] R.M. Guo, W.M. Xu, J.C. Lin, L.Q. Mo, X.X Hua, P.X. Chen, K. Wu, D.D. Zheng, J.Q. Feng,
830 Activation of the p38 MAPK/NF- κ B pathway contributes to doxorubicin-induced inflammation and
831 cytotoxicity in H9c2 cardiac cells. *Mol. Med. Rep.* (2013), 603-8.
832 <https://doi.org/10.3892/mmr.2013.1554>.

- 833 [64] S.F. Liu, A.B. Malik, NF-kappa B activation as a pathological mechanism of septic shock and
834 inflammation. *Am. J. Physiol. Lung Cell. Mol. Physiol.* (2006), 622-645.
835 <https://doi.org/10.1152/ajplung.00477.2005>.
- 836 [65] F. Schneider, C. Marban, G. Ajob, S. Helle, M. Guillot, A. Launoy, Q. Maestraggi, F. Scavello, O.
837 Rohr, M.H. Metz-Boutigue, In Trauma Patients, the Occurrence of Early-Onset Nosocomial
838 Infections is Associated With Increased Plasma Concentrations of Chromogranin A. *Shock* (2018),
839 522-528. <https://doi.org/10.1097/SHK.0000000000001000>
- 840 [66] Y.C. Tien, J.Y. Lin, C.H. Lai, C.H. Kuo, W.Y. Lin, C.H. Tsai, F.J. Tsai, Y.C. Cheng, W.H. Peng,
841 C.Y. Huang, *Carthamus tinctorius* L. prevents LPS-induced TNFalpha signaling activation and cell
842 apoptosis through JNK1/2-NFkappaB pathway inhibition in H9c2 cardiomyoblast cells. *J.*
843 *Ethnopharmacol.* (2010), 505-13. <https://doi.org/10.1016/j.jep.2010.05.038>
- 844 [67] H. Yuan, C.N. Perry, C. Huang, E. Iwai-Kanai, R.S. Carreira, C.C. Glembotski, R.A. Gottlieb, LPS-
845 induced autophagy is mediated by oxidative signaling in cardiomyocytes and is associated with
846 cytoprotection. *Am. J. Physiol. Heart Circ. Physiol.* (2009), 470-9.
847 <https://doi.org/10.1152/ajpheart.01051.2008>.
- 848 [68] S. Lei, Y. Zhang, W. Su, L. Zhou, J. Xu, Z.Y. Xia, Remifentanil attenuates lipopolysaccharide-
849 induced oxidative injury by downregulating PKCβ2 activation and inhibiting autophagy in H9C2
850 cardiomyocytes. *Life Sci.* (2018),109-115. <https://doi.org/10.1016/j.lfs.2018.10.041>.
- 851 [69] W.L. DeLano, *The PyMOL molecular graphics system*. DeLano Scientific, Palo Alto, (2002).

